

Application of A\* algorithm for tortuosity and effective porosity estimation of 2D rock images

*Original*

Application of A\* algorithm for tortuosity and effective porosity estimation of 2D rock images / Panini, F., SALINA BORELLO, E., Peter, C., Viberti, D.. - ELETTRONICO. - (2022), pp. 519-530. (48th International Summer School-Conference "Advanced Problems in Mechanics" APM 2020 St. Petersburg, Russia - ONLINE June 21-26, 2020) [10.1007/978-3-030-92144-6\_39].

*Availability:*

This version is available at: 11583/2841148 since: 2022-09-05T09:59:07Z

*Publisher:*

Springer, Cham

*Published*

DOI:10.1007/978-3-030-92144-6\_39

*Terms of use:*

This article is made available under terms and conditions as specified in the corresponding bibliographic description in the repository

*Publisher copyright*

(Article begins on next page)

XLVIII INTERNATIONAL  
SUMMER SCHOOL – CONFERENCE  
ADVANCED PROBLEMS IN MECHANICS

JUNE 21–26, 2020,  
ONLINE

APM 2020 PROGRAMME



<http://apm-conf.spb.ru>



**POLYTECH**  
Peter the Great  
St. Petersburg Polytechnic  
University



*Russian Academy of Sciences*



# Application of A\* algorithm for tortuosity and effective porosity estimation of 2D rock images

Filippo Panini<sup>1</sup>[0000-0002-5562-1336], Eloisa Salina Borello<sup>1</sup>[0000-0001-6484-899X], Costanzo Peter<sup>1</sup>[0000-0003-2649-6422], Dario Viberti<sup>1</sup>[0000-0001-7253-3402]

<sup>1</sup> Politecnico di Torino, Turin 10129, Italy  
filippo.panini@polito.it

**Abstract.** Characterization and understanding of fluid flow phenomena in underground porous media at the micro and macro scales is fundamental in reservoir engineering for the definition of the optimal reservoir exploitation strategy. Laboratory analyses on rock cores provide fundamental macroscale parameters such as porosity, absolute and relative permeability and capillary pressure curves. In turn, macroscale parameters as well as flow behavior, are strongly affected by the micro geometrical features of the rock, such as pore structure, tortuosity and pore size distribution. Therefore, a thorough comprehension of single and multiphase flow phenomena requires analyses, observations and characterization at the micro scale. In this paper we focus on the analysis of a 2D binary image of a real rock thin section to characterize the pore network geometry and to estimate tortuosity, effective porosity and pore size distribution. To this end, a geometrical analysis of the pore structure, based on the identification and characterization of the set of the shortest geometrical pathways between inlets and outlets pairs, is implemented. The geometrical analysis is based on the A\* path-finding algorithm derived from graph theory. The results provided by the geometrical analysis are validated against hydrodynamic numerical simulation via the Lattice Boltzmann Method (LBM), which is well suited for simulating fluid flow at the pore-scale in complex geometries. The selected rock for this analysis is Berea sandstone, which is recognized as a standard rock for various applications such as core analysis and flooding experiment. Results show that the path-finding approach provides reasonable and reliable estimates of tortuosity and can be successfully applied for analyzing the distribution of effective pore radius, as well as for estimating the effective porosity.

**Keywords:** Tortuosity, Effective Porosity, Path-finding Algorithm, Lattice Boltzmann Method.

## 1 Introduction

An optimal reservoir exploitation strategy has to be defined taking into account of different aspects related to economical, technical and environmental issues [33] and requires a deep understanding of the fluid flow phenomena dominating the reservoir behavior. From the viewpoint of the description and understanding of the reservoir

dynamic behavior, all the information provided by technical disciplines (such as geology, geophysics, log interpretation, laboratory measurements of fluids and rock properties, well testing, reservoir engineering and geomechanics) have to be taken into account, compared, combined and properly integrated [5, 12, 30, 31, 32, 34, 40, 41, 44]. Furthermore, it is well known that any complex and nonlinear problem is affected by uncertainties. Therefore, the uncertainty associated to the interpretation provided by each discipline must be estimated [19, 42, 43] and, if possible mitigated by acquiring new and necessary information at all stages of reservoir life, even during the production stage of a mature field.

In this view, characterization and understanding of fluid flow phenomena in underground porous media at the micro and macro scales is a fundamental piece of information that can minimize the uncertainties and contribute to maximize reservoir characterization and understanding. In many cases, the flow mechanism can be understood from pore-scale phenomena, allowing predictions at the macro-scale, which can then be compared with experimental results [4]. At the macro-scale, the fluid flow is modeled by averaging the microscopic continuity and momentum equations over a representative elementary volume (REV) [4] and the porous medium is parameterized mainly by porosity and permeability [14]; the fundamental equation of fluid motion in porous media under the assumption of small Reynolds numbers is Darcy's equation [4]:

$$\mathbf{u} = -\frac{\mathbf{k}}{\mu} \nabla P \quad (1)$$

where  $\mathbf{u}$  is the Darcy's velocity,  $\mathbf{k}$  is the permeability tensor,  $\mu$  the viscosity and  $\nabla P$  the pressure gradient.

Porous media are complex materials characterized by a chaotic structure and tortuous fluid flow, with pore and grains dimension varying over a wide range [14]. To address the crooked fluid paths of pore structure, the concept of tortuosity ( $\tau$ ) was introduced [9]. Two main types of tortuosity are defined in the literature: geometrical tortuosity ( $\tau_g$ ) and hydraulic tortuosity ( $\tau_h$ ). The geometrical tortuosity is defined as the shortest length between inflow and outflow points that avoids the solid obstacles divided by the distance between inlet and outlet [1, 11]. The hydraulic tortuosity is defined as the effective path length taken by the fluid divided by the length of the porous material measured along the flow direction [9]. Since the fluid flow path is always greater than the shortest geometrical path, hydraulic tortuosity is always greater than the geometrical tortuosity [11, 14]. For a complete review on the definitions of tortuosity, the reader can refer to [11] and to [14].

To account for pore space interconnections affected by the flow, the effective porosity ( $\phi_e$ ) was introduced; this property is defined as the percentage of conductive pore space with respect to the bulk volume [21]:

$$\phi_e = \frac{V_{flow}}{V_b} \quad (2)$$

where  $V_b$  is the bulk volume and  $V_{flow}$  is the portion of volume contributing to the fluid flow.

The impact of pore network geometry on the flow behavior is well recognized. In the literature, several analytical expressions have been provided to link permeability to the pore structure as a function of porosity (or effective porosity), tortuosity and grain or pore dimension. One of the most used expressions is the Kozeny-Carman equation [9,47]:

$$k = \frac{\phi r_H^2}{c\tau^2} \quad (3)$$

where  $c$  is the Kozeny's constant and  $r_H$  is the hydraulic radius, which gives a measure of the average pore dimension and is defined as [4]:

$$r_H = \phi \frac{V_b}{A_w} \quad (4)$$

where  $A_w$  is the wetted surface.

Several authors discussed the geometrical analysis of the pore structure from 2D and 3D images. Lindquist et al. [24] discussed the medial axes method to analyze structure properties such as pore throat and pore body size distributions and geometric tortuosity of a 3D digitalized image. Later, Sun et al. [37] used a shortest path approach based on Dijkstra's algorithm to calculate the geometric tortuosity and connected porosity; then, they applied a multiscale method approach to upscale the permeability. Al-Raoush and Madhoun [2] presented an algorithm for calculating geometric tortuosity from 3D X-ray tomography images of real rocks based on a guided search for connected paths utilizing the medial surface of the void space of a 3D segmented image.

In this paper we estimate tortuosity, effective porosity and permeability from a 2D binary images of rocks. To this end, we applied an approach based on geometrical analysis, developed based on a A\* path-finding procedure taken from the graph theory, of the porous medium. This approach was validated by numerical simulation via the Lattice Boltzmann Method (LBM). We report the results referred to a 2D image of Berea sandstone. Even if not reported here, a preliminary validation of the methodologies was carried out on a set of simplified synthetic cases for which the true value of the parameters of interest was analytically computed [45].

## 2 Methodology description

Starting point for the presented methodology is a 2D binary image of a rock section. Such data can be obtained by image processing of the Scanning Electron Microscopy (SEM) image of a thin section or the slice of an X-ray micro-tomography image. In this paper we analyzed a binary image of Berea sandstone taken from [8]. On the 2D binary image we analyzed the pore structure in terms of pathways accessible by fluid flow in single-phase conditions and calculated the associated parameters: tortuosity, effective porosity and permeability. Two different approaches were applied to assess pathways: geometrical and hydrodynamic. The pore structure analysis was completed by calculation of pore radius variations along the path compared with the hydraulic radius.

## 2.1 Geometrical path calculation

The pore structure of a binary 2D image is analyzed through a path-finding method based on graph representation. To this end, a set of inlets  $n_{in}$  and outlets  $n_{out}$  are placed along the inner and outer boundaries of the image of the porous domain orthogonal to the main flow direction (X or Y); the centroids of the pixels are used as reference grid node locations. These locations represent the points where the fluid enters and potentially leaves the porous system respectively.

The shortest pathway between each couple of inlet-outlet points is obtained through the A\* algorithm [18, 28]. A\* is based on a cost function  $f(n)$  to determine the optimal path between two nodes:

$$f(n) = g(n) + h(n) \quad (5)$$

where  $n$  indicates the considered node,  $g(n)$  the incremental distance from the considered node to the initial node and  $h(n)$  is a heuristic function used to obtain a prior estimation to reach the target from the considered node.

The process of obtaining the optimal shortest path is achieved by steps. Starting at the initial node, the cost function  $f(n)$  is calculated at each adjacent nodes in order to identify the one having the minimum cost which will be used as reference for the next calculation. This process is progressively repeated until the target is reached. The output is represented as a graph  $G = (N, E)$  with  $N$  being a set of nodes with  $X - Y$  coordinates while  $E$  the edges connecting the nodes (Fig. 1).

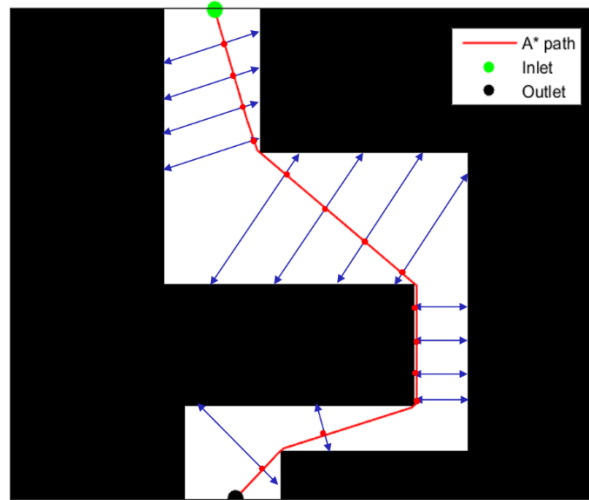


**Fig. 1.** Schematic of pore size and effective porosity estimation from path-finding approach.

## 2.2 Hydraulic path calculation

Hydrodynamic paths were obtained as a result of numerical simulation of single-phase fluid flow at the pore-scale. To this end, we implemented a discrete mesoscopic computational method based on the Lattice Boltzmann Method (LBM). LBM has been shown to be a powerful technique for the computational modeling of a wide variety of complex fluid flow problems including single and multiphase flows in complex geometries and porous media [8, 16]. The use of the LBM to evaluate the hydraulic tortuosity in synthetic porous media was presented by [27]. The LBM belongs to the family of discrete mesoscopic computational methods; unlike the conventional CFD methods, which numerically solve the Navier-Stokes (N-S) set of partial differential equations, the LBM solves the discrete lattice Boltzmann equation (LBE):

$$f_i(\mathbf{x} + \mathbf{v}_i, t + \Delta t) - f_i(\mathbf{x}, t) = \Omega_i(f_i(\mathbf{x}, t)) \quad (6)$$

where  $f_i$  is the density distribution function,  $\mathbf{v}_i$  the lattice velocity and  $\Omega_i$  the collision operator. The fluid is modeled as consisting of fictive particles which perform consecutive streaming and collision processes over a discrete reticular grid called lattice mesh [17]. The propagation and interaction of the particles is simulated in terms of the time evolution of the density distribution function, representing an ensemble average of the particle distribution. The flow properties such as velocity, pressure or fluid density can be derived from the moments of the density distribution function. The rules governing the collisions are designed such that the time-average motion of the particles is consistent with the macroscopic hydrodynamics. Collision rules constitutes a simplified mesoscopic kinetic model based on a Boltzmann-type equation that incorporate only the essential physics of microscopic or mesoscopic processes, avoiding to follow each particle as in molecular dynamics simulations [46]. Due to its particulate nature and local dynamics, the LBM has several advantages over other conventional CFD methods, especially in dealing with complex boundaries, incorporating of microscopic interactions, and parallelization of the algorithm [36]. The implementation adopted in this paper for single-phase flow simulation in porous media is based on a single-relaxation time (SRT) approximation of the collision operator, called Bhatnagar-Gross-Krook model (BGK) [7]:

$$\Omega_i = -\omega\Delta t[f_i(\mathbf{x}, t) - f_i^{eq}(\mathbf{x}, t)] \quad (7)$$

where  $\omega$  is the inverse of the relaxation time and  $f_i^{eq}$  the density distribution function at the equilibrium. The nine-velocity square lattice model D2Q9 was adopted to discretize the domain. At the fluid-solid interface, no-slip condition was imposed via halfway bounce-back [21]. Fixed pressure gradient between inlet and outlet was assumed as the boundary condition, which was implemented via the non-equilibrium bounce-back approach [48].

### 2.3 Characterization of pore structure

A quantitative characterization of the porous medium is carried out through the estimation of a series of parameters: pore size, tortuosity, effective porosity and permeability. In the following we will not parametrize the pore structure in terms of pore throat and pore body; we will refer to the local aperture between the pore walls as pore size or to the semi-aperture as pore radius.

Along the geometrical pathways identified by the A\* algorithm, the pore size is calculated at each node location by measuring the extension of the pore section length orthogonal to the local path direction (Fig. 1). The local pore size estimation allows monitoring the pore radius ( $r_p$ ) evolution along each detected path. This information can be used for reconstructing 3D porous geometries [29] or for comparative analysis with hydrodynamic data.

The output is also analyzed by a statistical representation of the pore radius distribution of the sample, which is compared with the hydraulic radius ( $r_H$ ). The hydraulic radius for a 2D section is defined as [45]:

$$r_H = \phi \frac{A_b}{P_w} \quad (8)$$

where  $A_b$  is the bulk area of the sample and  $P_w$  is the wetted perimeter, i.e. the interface between grains and void, which can be easily calculated by image processing routine; we used the Image Processing Toolbox of MATLAB [26].

The geometrical tortuosity  $\tau_g$  within a porous medium, in a given flow direction ( $dir$ ), is calculated through the ratio between the average of the shortest pathway lengths in that direction ( $\langle L_{sh,dir} \rangle$ ) by the length of the system domain along the fluid direction ( $L_{dir}$ ) [14]:

$$\tau_{g,dir} = \frac{\langle L_{sh,dir} \rangle}{L_{dir}} \quad (9)$$

where  $\langle L_{sh,dir} \rangle$  is calculated as the average of the shortest pathway lengths calculated.

Hydraulic tortuosity was defined by Carman [9] as the ratio of the average length of the fluid paths divided by the length of the sample:

$$\tau_h = \frac{\langle L_h \rangle}{L} \quad (10)$$

Koponen et al. [20] suggested to estimate tortuosity in a fixed direction from the velocity field simulated with a CFD numerical simulator as:

$$\tau_{h,dir} = \frac{\langle |v| \rangle}{\langle v_{dir} \rangle} \quad (11)$$

where  $|v|$  is the absolute value of the local flow velocity,  $v_{dir}$  is the directional component of that velocity and  $\langle \rangle$  denotes the spatial average over the pore space. We made use of a numerical simulator based on the Lattice Boltzmann Method (LBM) to simulate the fluid flow in the porous media at the pore-scale and obtain the velocity field and calculate the hydraulic tortuosity ( $\tau_h$ ) with Eq. 11. We also verified the invariance of calculated tortuosity with respect to the variation of the applied pressure

gradient until laminar flow conditions are guaranteed ( $Re \leq 2$ ) [3], where  $Re$  is the Reynolds number.

In [45], we proposed a purely geometrical calculation of the effective porosity based on path-finding:

$$\phi_{eg} = \frac{N_{pp}}{N_{px}} \quad (12)$$

where  $N_{pp}$  is the number of image pixels belonging to the portion of pore channels crossed by a pathway (in X or Y direction) and  $N_{px}$  the total number of image pixels.

The permeability can be calculated both applying the Darcy's law ( $k_h$ ) and the Kozeny-Carman equation ( $k_{KC,g}$ ). The subscript  $h$  indicate that in the first case the permeability is calculated by using the outputs of the numerical simulation, while in the second case the subscript  $g$  indicate that values obtained by geometric approach were used as inputs in the Kozeny-Carman equation. In the first case, the Darcy's velocity is computed from the hydrodynamical simulation velocity ( $\mathbf{v}$ ) as [15]:

$$\mathbf{u} = \frac{1}{A} \int_A \mathbf{v}(x, y) dA \quad (13)$$

Then the permeability is estimated as:

$$k_{h,dir} = -\frac{u_{dir}\mu}{\nabla_{dir}P} \text{ where } dir = x, y \quad (14)$$

In the second case, the Kozeny-Carman equation (Eq. 3) was modified substituting the porosity with the effective porosity calculated as in Eq. 12 and the tortuosity with the geometrical tortuosity calculated as in Eq. 9, obtaining an estimate of permeability only based on a geometrical analysis of the porous medium:

$$k_{KC,g,dir} = \frac{\phi_{eg} r_H^2}{c \tau_{g,dir}^2} \quad (15)$$

where in our case  $c = 5$  [4].

### 3 Case study: 2D image of Berea sandstone

The geometrical and hydrodynamic characterization is carried out on an image obtained from thin sections of 3D samples of Berea sandstone ( $D_{50} = 23 \mu m$  [11]). Berea sandstone is characterized by high difference between pore throat and pore body dimension [10] and the high porosity and permeability values make this rock a potential source of oil and natural gas. The image used in this study is reported in Fig. 2. The image dimensions are  $769 \times 624 \text{ px}^2$  (resolution of 4120 ppcm) and the 2D porosity calculated from the image is 0.3.

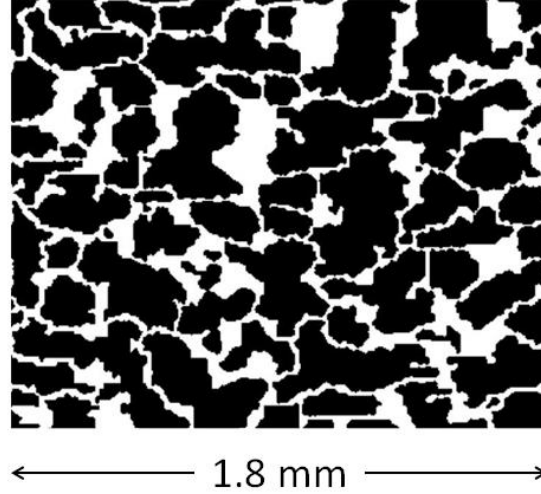


Fig. 2. 2D image of Berea sandstone

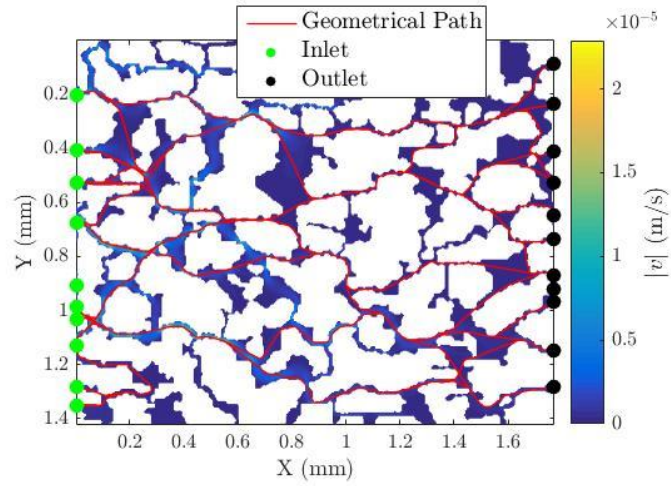
### 3.1 Results and discussion

In order to observe hydrodynamic behavior, the smallest pore size should be 4–5 lattice units [36]. The parameters adopted for the numerical simulations are:  $n_x=1706$  l.u.,  $n_y=1367$  l.u.,  $\Delta x=1.04 \mu m$  /l.u. The fluid used for the numerical simulation has the following properties: viscosity 0.5 cP, density 1050 kg/m<sup>3</sup>. A pressure gradient of 100 Pa/m was applied between inlet and outlet. Laminar flow occurs ( $Re=3.18E-04$ ). The case study was analyzed separately in the X and Y directions to assess eventual discrepancy in tortuosity and permeability which indicates anisotropy in the medium.

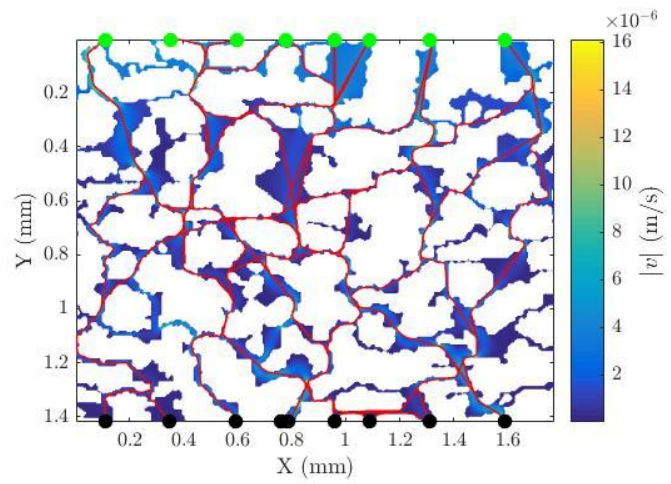
Results are summarized in Table 1. Fig. 3 compares the shortest paths obtained with the A\* algorithm (red lines) with the velocity map resulting from the numerical simulation. The pore zones contributing to the flow and used for the calculation of the effective porosity are represented in red in Fig. 4. In Fig. 5 the pore size distribution (Fig. 5a) and the pore size variation along a path (Fig. 5b) are compared with the hydraulic radius.

Table 1. Comparison of results obtained with the geometrical and hydrodynamic approaches

	Geometric	Hydrodynamic
$\tau_x$ (-)	1.250	1.416
$\tau_y$ (-)	1.437	1.542
$\phi_e$ (-)	0.277	0.256



(a)



(b)

**Fig. 3.** Simulated velocity map ( $|v|$ ) vs. detected geometrical paths considering flow in the X (a) and Y (b) directions.

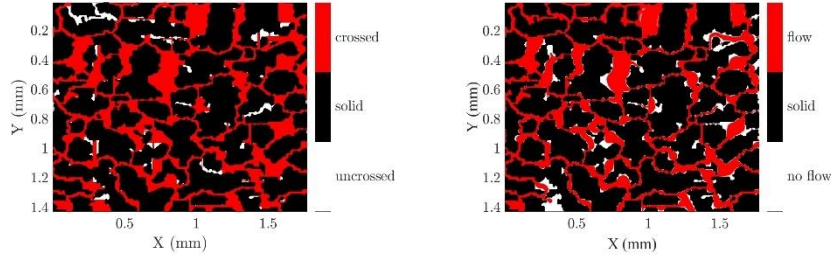


**Fig. 4.** Pore volume interested by flow (red) and dead zones (white) identified by applying the path-finding algorithm (on the left) vs. a cutoff on the simulated velocity (on the right)

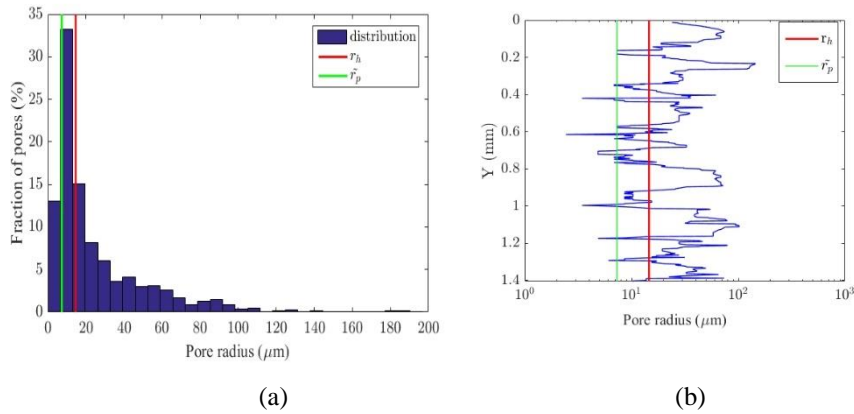


**Fig. 5.** Pore radius estimation from the path-finding approach: (a) pore radius distribution compared with hydraulic radius (red line); (b) pore radius variation along a single vertical path, compared with the mode of the pore radius along the selected path (green line) and the hydraulic radius (red line).

Tortuosity values calculated with the two methods (Tab. 1) are comparable (the discrepancy is lower than 10%) and the geometrical tortuosity is slightly smaller than the hydraulic tortuosity, as expected [14]. Comparing our results with literature, the tortuosity results are coherent with the gamma-shaped distribution with a minimum value of 1.07 and a most probable value close to 2, reported in [24] and just below the range of 1.6–2.8 reported in [38]. The pore radius distribution obtained by path finding algorithm appears to be reliable. The distribution in Fig. 5a is in good agreement with the literature: 31% of pore throats diameter of about  $10 \mu\text{m}$  [23];  $5 \mu\text{m}$  as the most frequent pore throat radius [29]; 37% of relative pore volume characterized by 7–10  $\mu\text{m}$  of pore radius [35]. Reasonable agreement (order of magnitude) is observed

between the hydraulic radius ( $r_H = 14.6 \mu m$ ) and the mode of pore radius distribution ( $\tilde{r}_p = 7.29 \mu m$ ) obtained by the path-finding approach (Fig. 5), thus suggesting that hydraulic radius formula (Eq. 8) is reasonably representative of the effective pore radius of the sample.

The values of permeability calculated with hydrodynamic approach ( $k_h$ ) through Darcy's law (Eq. 14) are of the order of magnitude of 1 D and comparable with those reported in [8]. As we expected [25], the permeability evaluated with the geometrical approach ( $k_{KC,g}$ ) through Kozeny-Carman equation (Eq. 15) was significantly higher than  $k_h$ , being of the order of magnitude of 6-7 D. It was observed that, if in Kozeny-Carman equation the pore radius mode ( $\tilde{r}_p$ ) is adopted instead of the hydraulic radius ( $r_H$ ) the resulting permeability reduces to about 1.5 D, becoming comparable with the hydrodynamic one. Further investigation will be carried out in future works.

## 4 Conclusions

In this paper we adopt a geometrical analysis based on a path-finding algorithm for the characterization of the pore network geometry and connectivity of 2D binary images of rock samples representative of real geological formations. In order to validate the results, we used a hydrodynamic numerical simulator based on the LBM and compared the results. Results showed that even if hydrodynamic simulation was more accurate in reproducing the flow behavior, the path-finding approach could give reasonable estimates of tortuosity and could also be successfully applied for analyzing the distribution of effective pore radius, as well as for estimating the effective porosity and for giving a reasonable order of magnitude of permeability.

## References

1. Adler, P.: Porous Media: Geometry and Transports. Elsevier (2013).
2. Al-Raoush, R. I., & Madhoun, I. T.: TORT3D: A MATLAB code to compute geometric tortuosity from 3D images of unconsolidated porous media. Powder technology, 320, 99-107 (2017).
3. Aminpour, M., Galindo-Torres, S. A., Scheuermann, A., & Li, L.: Pore-scale behavior of Darcy flow in static and dynamic porous media. Physical Review Applied, 9(6), 064025 (2018).
4. Bear, J.: Dynamics of Fluids in Porous Media. Courier Corporation (2013).
5. Benetatos, C., Viberti, D. Fully integrated hydrocarbon reservoir studies: Myth or reality? : American Journal of Applied Sciences, 7 (11), pp. 1477-1486. DOI: 10.3844/ajassp.2010.1477.1486 (2010).
6. Blunt, M. J.: Flow in porous media—pore-network models and multiphase flow. Current opinion in colloid & interface science, 6(3), 197-207 (2001).
7. Bhatnagar, P. L., Gross, E. P., & Krook, M.: A model for collision processes in gases. I. Small amplitude processes in charged and neutral one-component systems. Physical review, 94(3), 511 (1954).

8. Boek, E. S., & Venturoli, M.: Lattice-Boltzmann studies of fluid flow in porous media with realistic rock geometries. *Computers & Mathematics with Applications*, 59(7), 2305-2314 (2010).
9. Carman, P. C.: Fluid flow through granular beds. *Trans. Inst. Chem. Eng.*, 15, 150-166 (1937).
10. Churcher, P. L., French, P. R., Shaw, J. C., & Schramm, L. L.: Rock properties of Berea sandstone, Baker dolomite, and Indiana limestone. In *SPE International Symposium on Oilfield Chemistry*. Society of Petroleum Engineers (1991, January).
11. Clennell, M. B.: Tortuosity: a guide through the maze. Geological Society, London, Special Publications, 122(1), 299-344 (1997).
12. Fokker P., Salina Borello E., Verga F., Viberti D.: Harmonic Pulse Testing for Well Performance Monitoring. *Journal of Petroleum Science and Engineering*. Elsevier. Vol.162 pp.446-459 doi: <https://doi.org/10.1016/j.petrol.2017.12.053> (2018).
13. Gao, Z., & Hu, Q.: Investigating the effect of median pore-throat diameter on spontaneous imbibition. *Journal of Porous Media*, 18(12) (2015).
14. Ghanbarian, B., Hunt, A. G., Ewing, R. P., & Sahimi, M.: Tortuosity in porous media: a critical review. *Soil science society of America journal*, 77(5), 1461-1477 (2013).
15. Guibert, R., Nazarova, M., Horgue, P., Hamon, G., Creux, P., & Debenest, G.: Computational permeability determination from pore-scale imaging: sample size, mesh and method sensitivities. *Transport in Porous Media*, 107(3), 641-656 (2015).
16. Guo, Z., & Zhao, T. S.: Lattice Boltzmann model for incompressible flows through porous media. *Physical review E*, 66(3), 036304 (2002).
17. Guo, Z., & Shu, C.: Lattice Boltzmann method and its applications in engineering (Vol. 3). World Scientific (2013).
18. Hart, P. E., Nilsson, N. J., & Raphael, B.: A formal basis for the heuristic determination of minimum cost paths. *IEEE transactions on Systems Science and Cybernetics*, 4(2), 100-107 (1968).
19. Horne R.N.: Uncertainty in Well Test Interpretation. SPE-27972-MS. University of Tulsa Centennial Petroleum Engineering Symposium, 29-31 August, Tulsa, Oklahoma. DOI: 10.2118/27972-MS (1994).
20. Koponen, A., Kataja, M., & Timonen, J. V.: Tortuous flow in porous media. *Physical Review E*, 54(1), 406 (1996).
21. Koponen, A., Kataja, M., & Timonen, J.: Permeability and effective porosity of porous media. *Physical Review E*, 56(3), 3319 (1997).
22. Ladd, A. J.: Numerical simulations of particulate suspensions via a discretized Boltzmann equation. Part 1. Theoretical foundation. *Journal of fluid mechanics*, 271, 285-309 (1994).
23. Li, K., & Horne, R. N.: Fractal characterization of the geysers rock. In *Proceedings of the GRC 2003 annual meeting* (2003, October).
24. Lindquist, W. B., Lee, S. M., Coker, D. A., Jones, K. W., & Spanne, P. Medial axis analysis of void structure in three-dimensional tomographic images of porous media. *Journal of Geophysical Research: Solid Earth*, 101(B4), 8297-8310 (1996).
25. Lock, P. A.: Estimating the permeability of reservoir sandstones using image analysis of pore structure. Doctoral dissertation, Department of Earth Science and Engineering, Imperial College (2001).
26. Mathworks: Image Processing Toolbox User's Guide (2017).
27. Matyka, M., Khalili, A., & Koza, Z.: Tortuosity-porosity relation in porous media flow. *Physical Review E*, 78(2), 026306 (2008).
28. Nilsson, N. J.: Principles of artificial intelligence. Morgan Kaufmann (2014).

29. Øren, P. E., & Bakke, S.: Reconstruction of Berea sandstone and pore-scale modelling of wettability effects. *Journal of petroleum science and engineering*, 39(3-4), 177-199 (2003).
30. Panini, F., Onur, M., & Viberti, D.: An Analytical Solution and Nonlinear Regression Analysis for Sandface Temperature Transient Data in the Presence of a Near-Wellbore Damaged Zone. *Transport in Porous Media*, 129(3), 779-810 (2019).
31. Peter C., Sacchi Q., Salina Borello E.: Study of reservoir production uncertainty using channel amalgamation. In *geingegneria ambientale e mineraria (GEAM)*. Pàtron Editore S.r.l, Vol. 146, n.3, pp. 53-64 (2015).
32. Peter C., Salina Borello E., Dalman R., Karamitopoulos P., Busschers F., Sacchi Q., Verga F.: Improved lithology prediction in channelized reservoirs by integrating stratigraphic forward modelling: towards improved model calibration in a case study of the Holocene Rhine-Meuse fluvio-deltaic system. *Computers and Geosciences*. Vol. 141. Elsevier. <https://doi.org/10.1016/j.cageo.2020.104517> (2019).
33. Rocca, V., Viberti, D.: Environmental Sustainability Of Oil Industry. *American Journal of Environmental Sciences*. Vol. 9. Pp. 210-217. ISSN:1553-345X. DOI: 10.3844/ajessp.2013.210.217 (2013).
34. Salina Borello E., Fokker P. A., Viberti D., Verga F., Hofmann H., Meier P., Min K.-B., Yoon K., and Zimmermann G.: Harmonic Pulse Testing for Well Monitoring: application to a fractured geothermal reservoir. *Water Resources Research*. AGU Publications. Wiley. Vol. 55, n. 6, pp. 4727-4744. <https://doi.org/10.1029/2018WR024029> (2019).
35. Shi, J. Q., Xue, Z., & Durucan, S.: Supercritical CO<sub>2</sub> core flooding and imbibition in Berea sandstone—CT imaging and numerical simulation. *Energy Procedia*, 4, 5001-5008 (2011).
36. Succi, S.: *The Lattice Boltzmann Method for Fluid Dynamics and Beyond*. Oxford University Press (2001).
37. Sun, W. C., Andrade, J. E., & Rudnicki, J. W.: Multiscale method for characterization of porous microstructures and their impact on macroscopic effective permeability. *International Journal for Numerical Methods in Engineering*, 88(12), 1260-1279 (2011).
38. Takahashi, M., Kato, M., Urushimatsu, Y.: Geometry of Pore Structure in Pressurized Berea Sandstone. *EUROCK2009 Rock Engineering in Difficult Ground Conditions*. International Society for Rock Mechanics and Rock Engineering (2009).
39. Timm, K., Kusumaatmaja, H., Kuzmin, A., Shardt, O., Silva, G., & Viggen, E.: *The lattice Boltzmann method: principles and practice* (2016).
40. Verga F., Viberti D., Salina Borello E.: A new insight for reliable interpretation and design of injection tests. In: *journal of petroleum science and engineering*, Elsevier, vol. 78, pp. 166-177. - ISSN 0920-4105 - doi: 10.1016/j.petrol.2011.05.002 (2011).
41. Verga F., Salina Borello E.: Unconventional well testing: a brief overview. In *geingegneria ambientale e mineraria (GEAM)*. Pàtron Editore S.r.l, Vol. 149, n.3, pp.45-54 (2016)
42. Viberti, D.: A rigorous mathematical approach for petrophysical properties estimation. *American Journal of Applied Sciences*, 7 (11), pp. 1509-1516. - ISSN 1546-9239. DOI: 10.3844/ajassp.2010.1509.1516 (2010).
43. Viberti, D., Verga, F.: An Approach for the Reliable Evaluation of the Uncertainties Associated to Petrophysical Properties, *Mathematical Geosciences*, Springer, Vol. 4, Issue 3, pp. 327-341. DOI 10.1007/s11004-011-9358-1 (2012).
44. Viberti D., Cossa A., Galli M.T., Pirrone M., Salina Borello E., Serazio C.: A novel approach to a quantitative estimate of permeability from resistivity log measurements. In *geingegneria ambientale e mineraria (GEAM)*. Pàtron Editore S.r.l, Vol. 155, n.3, pp. 17-24 (2018)

45. Viberti, D., Peter, C., Borello, E. S., & Panini, F.: Pore structure characterization through path-finding and Lattice Boltzmann simulation. *Advances in Water Resources*, 103609 (2020).
46. Tu, J., Yeoh, G. H., & Liu, C.: Some advanced topics in CFD. *Computational Fluid Dynamics*, 369-417 (2018).
47. Wyllie, M. R. J., & Spangler, M. B: Application of electrical resistivity measurements to problem of fluid flow in porous media. *AAPG Bulletin*, 36(2), 359-403 (1952).
48. Zou, Q., & He, X.: On pressure and velocity boundary conditions for the lattice Boltzmann BGK model. *Physics of fluids*, 9(6), 1591-1598 (1997).